MACF1 Mutations Encoding Highly Conserved Zinc-Binding Residues of the GAR Domain Cause Defects in Neuronal Migration and Axon Guidance

William B. Dobyns,[1,2,3,24,*] Kimberly A. Aldinger,[3,24] Gisele E. Ishak,[3,4,24] Ghayda M. Mirzaa,[1,3] Andrew E. Timms,[5] Megan E. Grout,[1] Marjolein H.G. Dremmen,[6,7] Rachel Schot,[8] Laura Vandervore,[8] Marjon A. van Slegtenhorst,[8] Martina Wilke,[8] Esmee Kasteleijn,[8] Arthur S. Lee,[9,10] Brenda J. Barry,[9] Katherine R. Chao,[10] Krzysztof Szczałuba,[11] Joyce Kobori,[12] Andrea Hanson-Kahn,[13,14] Jonathan A. Bernstein,[14] Lucinda Carr,[15] Felice D'Arco,[15] Kaori Miyana,[16] Tetsuya Okazaki,[17] Yoshiaki Saito,[17] Masayuki Sasaki,[18] Soma Das,[19] Marsha M. Wheeler,[20,21] Michael J. Bamshad,[1,20,21] Deborah A. Nickerson,[20,21] University of Washington Center for Mendelian Genomics,[21] Center for Mendelian Genomics at the Broad Institute of MIT and Harvard,[10] Elizabeth C. Engle,[9,10,22,23] Frans W. Verheijen,[8] Dan Doherty,[1,3,24] and Grazia M.S. Mancini[8,24,*]

To date, mutations in 15 actin- or microtubule-associated genes have been associated with the cortical malformation lissencephaly and variable brainstem hypoplasia. During a multicenter review, we recognized a rare lissencephaly variant with a complex brainstem malformation in three unrelated children. We searched our large brain-malformation databases and found another five children with this malformation (as well as one with a less severe variant), analyzed available whole-exome or -genome sequencing data, and tested ciliogenesis in two affected individuals. The brain malformation comprised posterior predominant lissencephaly and midline crossing defects consisting of absent anterior commissure and a striking W-shaped brainstem malformation caused by small or absent pontine crossing fibers. We discovered heterozygous de novo missense variants or an in-frame deletion involving highly conserved zinc-binding residues within the GAR domain of MACF1 in the first eight subjects. We studied cilium formation and found a higher proportion of mutant cells with short cilia than of control cells with short cilia. A ninth child had similar lissencephaly but only subtle brainstem dysplasia associated with a heterozygous de novo missense variant in the spectrin repeat domain of MACF1. Thus, we report variants of the microtubule-binding GAR domain of MACF1 as the cause of a distinctive and most likely pathognomonic brain malformation. A gain-of-function or dominant-negative mechanism appears likely given that many heterozygous mutations leading to protein truncation are included in the ExAC Browser. However, three de novo variants in MACF1 have been observed in large schizophrenia cohorts.

Microtubules (MTs) and filamentous actin form key structural components of the cytoskeleton, a dynamic intracellular structure that is essential for several basic cell functions, including migration, the formation of cellular processes (including axons and dendrites), axonal guidance, and vesicular trafficking. Mammalian genomes contain two spectraplakins—MACF1 (also known as ACF7) and DST (also known as BPAG1)—that function as actin-MT cross-linkers and essential integrators and modulators of cytoskeletal processes.[1–3]

MACF1 is a large gene that expresses many isoforms, several of which are brain specific, through alternative splicing. The N terminus of the major isoforms contains two calponin-homology (CH) domains that bind actin, a plakin domain, and a long spectrin-repeat rod domain that confers flexibility. The C terminus of all isoforms functions as a MT binding domain and contains two calcium-binding EF-hand domains, a zinc-binding GAR (growth-arrest specific 2 or Gas2-related) domain, a positively charged Gly-Ser-Arg (GSR) region, and an EB1-binding SxIP domain.[1–3]

[1]Department of Pediatrics, University of Washington, Seattle, WA 98195, USA; [2]Department of Neurology, University of Washington, Seattle, WA 98195, USA; [3]Center for Integrative Brain Research, Seattle Children's Research Institute, Seattle, WA 98101, USA; [4]Department of Radiology, University of Washington, Seattle, WA 98195, USA; [5]Center for Developmental Biology and Regenerative Medicine, Seattle Children's Research Institute, Seattle, WA 98101, USA; [6]Department of Radiology, Erasmus MC University Medical Center, Rotterdam 3015 CN, the Netherlands; [7]Division of Pediatric Radiology, Sophia Children's Hospital, Rotterdam 3015 CN, the Netherlands; [8]Department of Clinical Genetics, Erasmus MC University Medical Center, Rotterdam 3015 CN, the Netherlands; [9]Department of Neurology, Children's Hospital Boston and Harvard Medical School, Boston, MA 02115, USA; [10]Center for Mendelian Genomics at the Broad Institute of MIT and Harvard, Cambridge, MA 02142, USA; [11]Department of Medical Genetics, Medical University of Warsaw, Warsaw 02-106, Poland; [12]Department of Genetics, Permanente Medical Group, San Jose, CA 95123, USA; [13]Department of Genetics, Stanford School of Medicine, Stanford, CA 94305, USA; [14]Department of Pediatrics, Stanford School of Medicine, Stanford, CA 94305, USA; [15]Department of Neuroradiology, Great Ormond Street Hospital for Children NHS Foundation Trust, London WC1N 3JH, UK; [16]Department of Pediatrics, Japanese Red Cross Medical Center, Shibuya, Tokyo, Japan; [17]Division of Child Neurology, Department of Brain and Neurosciences, Faculty of Medicine, Tottori University, Yonago, Tottori, Japan; [18]Department of Child Neurology, National Center Hospital, National Center of Neurology and Psychiatry, Tokyo, Japan; [19]Department of Human Genetics, University of Chicago, Chicago, IL 60637, USA; [20]Department of Genome Sciences, University of Washington, Seattle, WA 98195, USA; [21]University of Washington Center for Mendelian Genomics, Seattle, WA 98195, USA; [22]Department Ophthalmology, Children's Hospital Boston and Harvard Medical School, Boston, MA 02115, USA; [23]Howard Hughes Medical Institute, Chevy Chase, MD 20815, USA
[24]These authors contributed equally to this work
*Correspondence: wbd@uw.edu (W.B.D.), g.mancini@erasmusmc.nl (G.M.S.M.)
https://doi.org/10.1016/j.ajhg.2018.10.019.

This work began after we recognized a complex brain malformation consisting of lissencephaly (LIS), a rare brainstem malformation with deficient midline crossing, and multiple developmental deficits including severe intellectual disability and epilepsy in three unrelated children during intergroup reviews. We next searched our large brain-malformation databases (~3,300 subjects) and identified the same pattern in another five children for a total of eight, including monozygotic twin sisters and one previously reported Japanese girl (Figures 1, 2, S1, and S2).[4]

Phenotype

According to our revised classification system for LIS,[5] the cortical malformation consists of diffuse pachygyria with thick cortex and a mild posterior gradient more severe than the anterior gradient; it varied from "thin" LIS with mildly thick cortex (7–10 mm) in six of eight individuals to classic LIS with very thick cortex (10–15 mm) in two of eight individuals. We found thin anterior commissures and mildly dysplastic hippocampi in all eight individuals and mildly thin corpus callosum in six of eight subjects.

The brainstem malformation consisted of severe dorso-ventral narrowing of the brainstem mostly in the pons and small ventral prominences on mid-sagittal images (Table 1 and Figures 1 and S1). On axial images, the lower midbrain and entire pons and medulla were narrow on the dorso-ventral axis with a prominent ventral midline cleft but were also very wide, resembling a thick "W" (or wide bird wings when turned upside down), on the right-left axis (see Figures 1B, 1F, and 1J). The base of the pons was small (4–5 mm) in three individuals, tiny (2–3 mm) in three individuals, and absent in two of eight individuals. Cranial nerves could be seen exiting from the ventral surface of both medial and lateral aspects of the dysplastic brainstem. Coronal 3D image reconstructions along the ventral brainstem showed absent or very sparse transverse pontine crossing fibers, uncovering the pyramidal tracts (Figures 2 and S2). The cerebellar vermis was moderately small in two individuals, mildly small in five individuals, and normal in one of eight individuals, whereas the cerebellar hemispheres were mildly small in seven individuals and normal in (the same) one individual. Reconstructed diffusion tensor imaging sequences in one boy (LR17-434) showed small superior cerebellar peduncles and absent anterior and posterior transverse pontine crossing fibers (Figure 3). Similar changes were shown in the previously reported Japanese child.[4]

All eight children had global developmental delay, severe intellectual disability, axial hypotonia (with limb spasticity in three of eight), and seizures (Table 2). The twin girls were non-verbal and had the most severe intellectual disability, as well as short stature and microcephaly (3–5 standard deviations below the mean), although their pregnancy had been complicated only by gestational diabetes and premature birth at 37 weeks of gestation. One girl spoke more than 40 single words, and another used an assistive language device; the remainder used few or no words. Growth was normal except for in the twins. Seizure types included infantile spasms in two individuals (which resolved after steroid treatment in one), myoclonic seizures in two individuals, and mixed partial and generalized seizures in the remaining four children. Involuntary movements were seen in three of eight individuals, and stereotypies were observed in two others. Cranial-nerve deficits consisted of dysphagia in four individuals, asymmetric facial movements in one individual, strabismus in three individuals, and limited ocular adduction in the previously reported child who improved by 5 years.[4] Cortical visual impairment was diagnosed in two children, and left optic-nerve hypoplasia was diagnosed in one, whereas hearing was normal in all. One individual had poor temperature regulation plus a neurogenic bladder and bowel attributed to spinal-cord dysfunction without structural abnormality. No consistent dysmorphic facial features were observed, and no other malformations were found, except for a ventricular septal defect that closed spontaneously in one child.

Genetic Analysis

The nine subjects were ascertained from multiple centers and enrolled in research after written informed consent was provided under protocols approved by institutional review boards at Seattle Children's Hospital, the University of Washington, Boston Children's Hospital, and Erasmus University Medical Center. Blood or tissue samples were obtained and genomic DNA was extracted according to standard protocols. Whole-exome sequencing was performed in six trios and one proband in seven different laboratories with sequencing parameters that varied modestly across centers and center-specific pipelines (Table S1 and Supplemental Material and Methods). These data were supplemented by whole-genome sequencing in two trios and Sanger sequencing of small critical regions in two probands (the second twin and LR18-077). When no coding changes were found, we looked for small deletions and duplications by manual inspection of read depth in regions where mutations were found in other affected individuals.

We found recurrent, heterozygous *de novo* missense variants involving three of the four highly conserved zinc-binding residues in the GAR domain of MACF1 in seven of eight children (Tables 1, 2, and S2 and Figure 4A). All variants were predicted to be deleterious: all CADD scores (28–34) were well above our standard cutoff of 15, and all PolyPhen-2 scores (0.995–0.999) were rated as probably damaging (Table S2). None of these variants were found in gnomAD.

No sequence variants of MACF1 were detected in the Japanese girl,[4] but manual inspection of read depth and analysis of exome sequence data with the GATK4 GenomeCNVCaller and of genome data with the Manta SV caller detected a 39.6 kb deletion of exons 62–93 (transcript MACF1-204), causing a predicted in-frame deletion from Ala5498 through Arg7150 (Table S2). This region
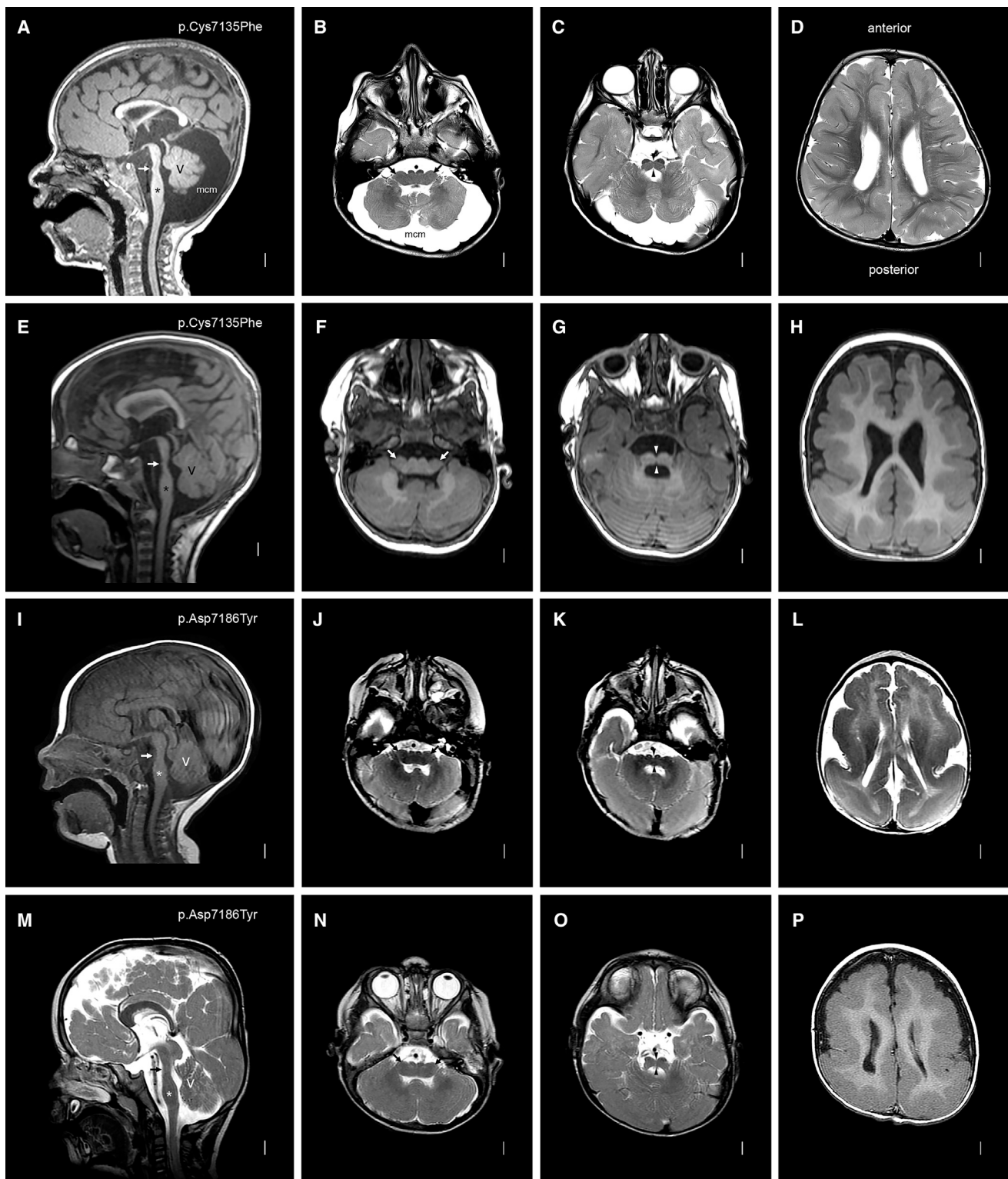
Figure 1. Brain MRI in Subjects with *MACF1* Zinc-Binding-Pocket Mutations

Images from mid-sagittal (far-left column) and three axial planes are shown from subjects LR14-088 (A–D), LR17-434 (E–H), LR16-306 (I–L), and LR17-450 (M–P). *MACF1* mutations are shown in the far-left column for each subject. The mid-sagittal images all show striking brainstem hypoplasia and dysplasia with a mildly narrow midbrain, a dramatically narrow pons with tiny (white arrows in A and E) or no (white arrows in I and M) bumps on the ventral surface, and a mildly thick medulla. The midline images also show a mildly thin and variably short corpus callosum and mild cerebellar vermis hypoplasia with mega-cisterna magna (A) or borderline vermis hypoplasia (E, I, and M). The medulla is very wide and flat—almost double the typical width—and has small pyramids visible on the ventral surface (arrows in B, F, J, and N). The pons is also very wide and flat with a deep ventral cleft in the midline (arrowheads in C, G, K, and O). Images of the cortex show diffuse mild (D and H) or severe (L and P) pachygyria with a posterior gradient more severe than the anterior gradient.
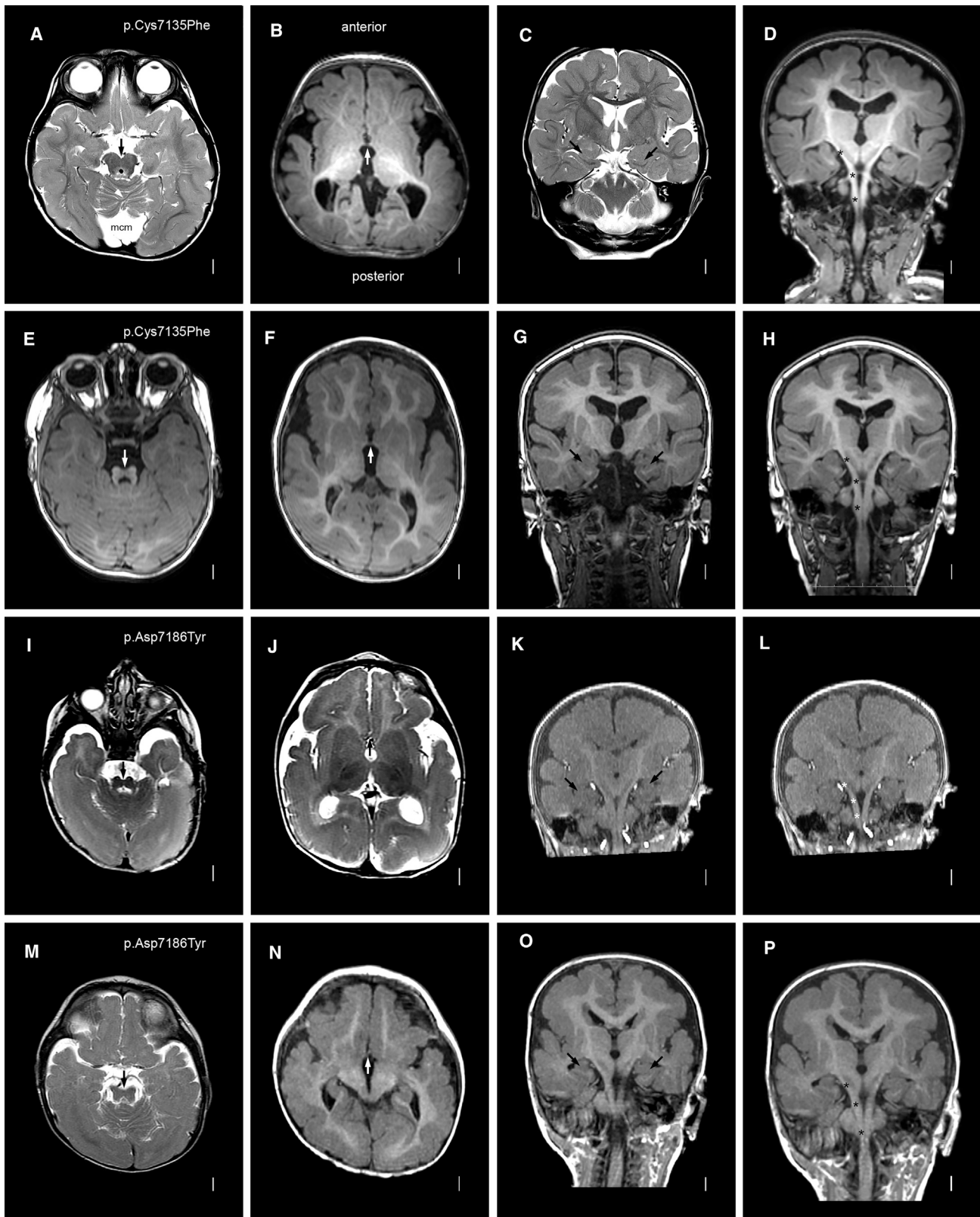
Figure 2. Brain MRI in Subjects with *MACF1* Zinc-Binding-Pocket Mutations: Additional Features

Axial (left two columns), coronal (third column), and reconstructed coronal (far-right column) images are shown for (the same as in Figure 1) subjects LR14-088 (A–D), LR17-434 (E–H), LR16-306 (I–L), and LR17-450 (M–P). *MACF1* mutations are again shown in the far-left column. The low midbrain or isthmus appears small and narrow with variably prominent superior cerebellar peduncles that

(legend continued on next page)

contains the last ten spectrin repeats, both EF-hand domains, and the first two zinc-binding residues: Cys7133 and Cys7135 (Figures 4A and S3). We designed primers flanking the predicted breakpoints to generate a 1.1 kb PCR product and defined breakpoint-flanking sequences that in the normal genome map to intronic sequences 39.6 kb apart: 5′-CCGGGGATTCTGTGTCATCTTAATA-3′–breakpoint–5′-TACAGTAAGCTGAGATCACACTGT-3′.

The GAR domain mediates MT binding and consists of a novel zinc-binding α-β fold composed of a five-stranded anti-parallel β sheet (β1–β5) flanked by N-terminal (α1) and C-terminal (α2) α helices that pack against the β sheet to form an α/β sandwich.[3] The α1-β1 loop and the C-terminal loop flanking α2 contain four highly conserved residues (Cys7133, Cys7135, Asp7186, and Cys7188 according to Ensembl sequence MACF1-204) that coordinate the bound zinc ion.[3] Our first seven subjects (including both twins) had recurrent missense variants involving three of the four zinc-binding residues. These are shown with both the standard NCBI sequence GenBank: NM_021090.5 and the longer Ensembl sequence MACF1-204 (Table S2). Hereafter, we refer only to the MACF1-204 transcript, which has been used for most functional studies.[3]

Genotype-Phenotype Analysis

Although the phenotypes were remarkably similar, we found several subtle differences. The two with p.Cys7135Phe had more severe hypoplasia of the anterior commissure, and the two with p.Asp7186Tyr had more severe LIS. The three with p.Cys7188Phe or p.Cys7188Gly and the child with the intragenic deletion had larger (3–4 mm) nodules representing residual pontine crossing fibers on the ventral surface of the pons; these were not seen or barely seen in the other four individuals (Table 1).

Protein Structure

We used the 3D modeling tool PyMOL to predict the effect of missense variants on protein structure of the GAR domain, which was previously resolved by molecular crystallography (Supplemental Material and Methods).[3] This region contains a sandwich structure and a divalent zinc-binding pocket formed by four highly conserved amino acids (three cysteines and one aspartate) that are invariant in spectraplakins and essential for MT binding. Substitutions involving these residues were predicted to significantly alter configuration of the zinc-binding pocket (Figure 4B), which supports experimental data showing compromised domain function when one of the cysteine residues is replaced by a serine and strongly supports pathogenicity of the protein variants, which most likely abrogate MT binding.[3]

Ciliogenesis

Studies using several cre drivers in mouse Macf1 knockouts demonstrated that loss of Macf1 in the retina, ependymal and cochlear sensory epilthelia, and mouse embryonic fibroblasts led to failure of cells to build cilia and disrupted apicobasal polarity in the retina, whereas heterozygous mutants had normal cilia.[6] We hypothesized that heterozygous variants in the GAR domain, if pathogenic, would also disrupt cilia formation, a key cellular function that can be tested in cells exiting mitosis after serum starvation.[7] We therefore tested cilium formation in skin fibroblasts from two subjects with MACF1 variants and compared it with that of mutant fibroblasts with known defects in cilium number and length (CEP290) or length alone (RTTN).[8]

Fibroblast lines from two control and five affected individuals with known mutations (two in MACF1, two in RTTN, and one in CEP290) were processed in parallel in duplicate or quadruplicate as previously described (Supplemental Material and Methods). In brief, cells were grown until they were 80% confluent, serum starved for 48 hr for the induction of cilium formation, fixed with methanol, incubated overnight with primary antibodies—mouse monoclonal anti-human acetylated tubulin (Sigma Aldrich T7451) and rabbit polyclonal anti-human gamma tubulin (Sigma Aldrich T3320)—and then incubated with secondary fluorescent antibodies for 1 hr. Cells with basal bodies (γ-tubulin positive) were scored for cilium length, defined as normal (>3 μm) or short (<3 μm), in four quadrants for each coverslip by one individual. Values indicate the average length ± SEM. Under these conditions, 50%–80% of cells grew cilia according to data from 100 experiments using multiple control fibroblast lines.

In contrast to the mouse homozygous mutants, human fibroblasts carrying MACF1 mutations made normal numbers of cilia, but a significantly larger percentage of cells had short cilia, indicating a length-control deficit similar to that of RTTN-mutant cells (Figure S4). Statistical tests for cilium formation and a length assay were performed with Prism 5 GraphPad.

Phenotype Variant

We also evaluated a ninth child with an overlapping disorder. Brain imaging studies in this girl showed mild, posterior predominant LIS similar to that of the children with variants in the GAR domain but only subtle brainstem dysplasia (Figures S1I–S1L and S2I–S2L). Within the C-terminal portion of the spectrin repeat domain of MACF1, we found a heterozygous de novo missense variant that lies within the genomic region deleted in the Japanese girl (Table S2). This region, designated SR4, contains residues 6,221–6,894 in Ensembl sequence MACF1-204 and

are smaller than seen in the molar-tooth malformation associated with Joubert syndrome (especially E, I, and M). The anterior commissures are thin (arrows in B, F, J, and N). The hippocampi are small and dysplastic (C, G, K, and O). The pyramidal tracts are easy to follow given the paucity of transverse pontine crossing fibers; a few are seen in the top two images (asterisks over the right pyramidal tracts in D and H), but none are seen in the lower images (asterisks in L and P).

Table 1. Brain Imaging Features of Individuals with *MACF1* Mutations

Subject ID	LIS with Brainstem Hypoplasia and Dysplasia								LIS Only
	LR14-088	LR17-434	LR16-306	LR17-450	LR04-067a1	LR04-067a2	LR18-077	LR18-070[4]	LR16-412
Protein Variants									
GenBank: NM_012090.5[a]	p.Cys5177Phe	p.Cys5177Phe	p.Asp5228Tyr	p.Asp5228Tyr	p.Cys5230Phe	p.Cys5230Phe	p.Cys5230Gly	deletion	p.Gly4706Arg
MACF1-204[b]	p.Cys7135Phe	p.Cys7135Phe	p.Asp7186Tyr	p.Asp7186Tyr	p.Cys7188Phe	p.Cys7188Phe	p.Cys7188Gly	deletion	p.Gly6664Arg
Cerebral Hemispheres									
LIS severity	PGY diffuse	PGY diffuse	PGY diffuse	PGY diffuse	PGY diffuse	PGY diffuse	PGY diffuse	PGY diffuse	PGY diffuse
LIS gradient	P > A	P > A	P > A	P > A	A = P	A = P	P > A	P > A	P > A
LIS cortical thickness	thin (4–7 mm)	thin (4–7 mm)	thick (10–15 mm)	thick (10–15 mm)	thin (4–7 mm)	thin (4–7 mm)	thin (4–7 mm)	thin (4–7 mm)	thin (4–7 mm)
Hippocampal dysplasia	yes	yes	yes	yes	yes	yes	yes	subtle	subtle
Thin white matter	yes	yes	yes	yes	yes	yes	yes	yes	yes
Commissures									
Anterior commissure	thin	thin	thin[c]	thin	borderline thin	borderline thin	thin	thin	normal
Corpus callosum	thin diffuse	thin diffuse	thin diffuse[d]	thin diffuse[d]	normal	normal	thin mild	normal	thin mild
Hippocampal commissure	normal	normal	normal	normal	normal	normal	normal	normal	normal
Optic chiasm	normal	normal	normal	normal	normal	normal	normal	normal	normal
Brainstem									
Thick tectum[e]	no	no	no	yes	no	no	no	no	no
Severe narrowing of pons	yes	yes	yes	yes	yes	yes	yes	yes	no
Wide pons and medulla	yes	yes	yes	yes	yes	yes	yes	yes	subtle
Base of pons	tiny	tiny	absent[c]	absent	small	small	small	tiny	no
Pontine hypoplasia	severe	severe (DTI)	severe	severe	moderate to severe	moderate to severe	moderate to severe	severe	no
Cerebellum									
Vermis hypoplasia	moderate	mild	mild	mild	mild	mild	moderate	no	normal
Hemisphere hypoplasia	moderate	mild	mild	mild	mild[f]	mild[f]	mild	no	normal
Foliar dysplasia	yes	yes	yes	yes	yes	yes	yes	yes	no

Abbreviations are as follows: A = P, anterior gradient same as posterior gradient; DTI, diffusion tensor imaging; LIS, lissencephaly; P > A, posterior gradient more severe than anterior gradient; PGY, pachygyria.
[a]GenBank: NM_012090.5 and transcript MACF1-203 (Ensembl: ENST00000361689.6).
[b]Transcript MACF1-204 (Ensembl: ENST00000372915.7).
[c]Low-resolution scan.
[d]Severe hypoplasia of splenium.
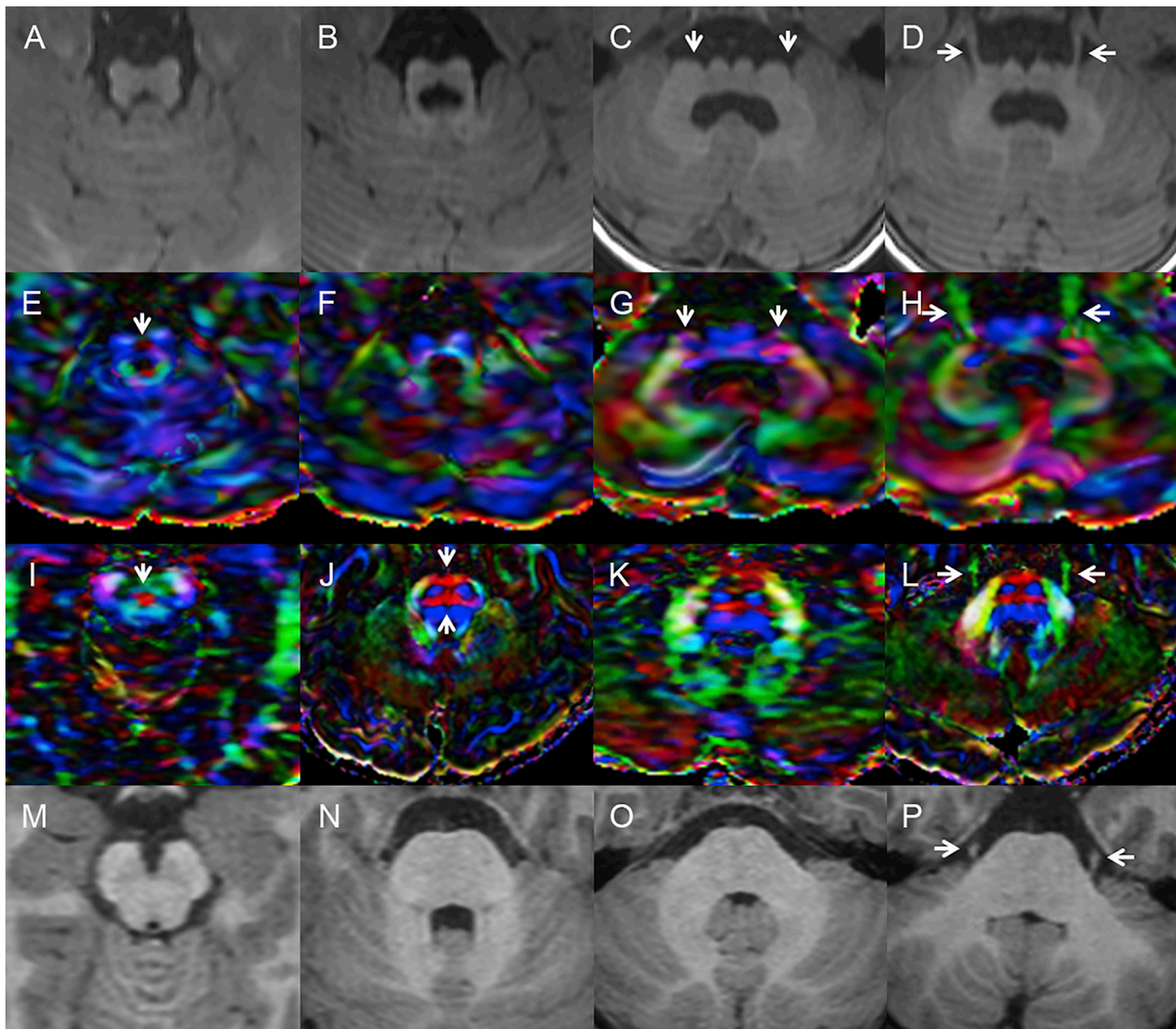[e]Fused colliculi.
[f]Right smaller than left.

Figure 3. Diffusion Tensor Imaging Confirms Defects in Midline Crossing Tracts

Axial T1-weighted magnetic resonance images and matched color-coded fractional-anisotropy maps from subject LR17-434 (A–H) and from a healthy control individual (I–P). Images at the level of the decussation of the superior cerebellar peduncles (first column) show a small midbrain (A) with the decussation represented as small (arrow in E) or medium-sized (arrow in I) red dots. Axial images through the upper pons (second column) demonstrate a ventral cleft in the midline of the small and dysplastic pons (B) and absence of the anterior and posterior transverse pontine fibers (F) in comparison with the healthy control individual (arrows in J). Axial images through the middle and low pons (third and fourth columns) demonstrate the narrow dorsal-ventral diameter and broad left-right axis of the brainstem (arrows in C and D) with descending and ventro-dorsal fibers (blue and green in G) seen in the far lateral pons (arrows pointing to blue and green tracts in G). The trigeminal nerves originate from the far lateral pons (arrows in D and H), a sharp contrast from the location of the trigeminal nerves in the control (arrows in L and P).

mediates binding to GSK3B as well as Axin and APC.[9] GSK3B regulates MACF1 binding to MTs and migration of pyramidal neurons to the cortical plate, suggesting a possible mechanism for the defect in neuronal migration.[1,9,10]

Our data demonstrate four missense mutations and one in-frame deletion in *MACF1*, which encodes zinc-binding residues in the MT-binding GAR domain, in eight children with a rare and distinctive brain malformation consisting of variable but usually mild LIS with a posterior gradient more severe than the anterior gradient, poorly formed hippocampi, an unusual brainstem malformation with very broad, flat pons and upper medulla, and midline-crossing defects involving the anterior commissure, transverse pontine crossing fibers, and probably pyramidal tracts.[4] The corpus callosum and cerebellum are less affected. Now being defined, the brain malformation is visually striking and most likely pathognomonic for *MACF1* mutations involving the GAR domain. We also identified a *de novo* variant in the MACF1 spectrin repeat domain in one girl with a similar type of LIS but only a subtle brainstem malformation.

Table 2. Clinical Features and Protein Variants in Individuals with *MACF1* Mutations

Subject ID	LIS with Brainstem Hypoplasia and Dysplasia								LIS Only
	LR14-088	LR17-434	LR16-306	LR17-450	LR04-067a1	LR04-067a2	LR18-077	LR18-070[4]	LR16-412
Protein Variants									
GenBank: NM_012090.5,[a]	p.Cys5177Phe	p.Cys5177Phe	p.Asp5228Tyr	p.Asp5228Tyr	p.Cys5230Phe	p.Cys5230Phe	p.Cys5230Gly	deletion[b]	p.Gly4706Arg
MACF1-204[c]	p.Cys7135Phe	p.Cys7135Phe	p.Asp7186Tyr	p.Asp7186Tyr	p.Cys7188Phe	p.Cys7188Phe	p.Cys7188Gly	deletion[b]	p.Gly6664Arg
Identity Data									
Sex	female	male	female	male	female	female	male	female	female
Ethnicity	C (Indian)	C (Dutch)	C (USA)	C (Polish)	C (Hispanic)	C (Hispanic)	C (Syrian)	A (Japanese)	C and A (Filipino)
Geographic origin	Mumbai	Rotterdam	Bay Area, CA	Warsaw	San Jose, CA	San Jose, CA	London	Saitama	Seattle, WA
Growth Data									
OFC at birth (SD)	36 cm (+1.1)	ND	ND	31 cm (−1)[d]	32.5 cm (−1.5)	ND	ND	33.5 cm (+0.4)	ND
Age at last exam	5 years	7.5 years	5.5 years	7 years	16 years	16 years	7 years	2.5 years	5 years
Weight (SD)	13.7 kg (−1.7)	28 kg (+1)	13.5 kg (+1.7)	14 kg (−3)	35.2 kg (−3)	29.0 kg (−4)	22 kg (−0.4)	10.0 kg (−1.6)	20.4 kg (+0.7)
Height (SD)	105 cm (−0.5)	128 cm (0)	103 cm (−1)	116 cm (−1)	150 cm (−2)	137 cm (−4)	50 cm (−2)	82.5 cm (−1.6)	107.9 cm (−0.1)
OFC (SD)	50.5 cm (0)	53 cm (+0.7)	45.5 cm (−1)	47 cm (+0.5)[e]	49.5 cm (−4)	47.7 cm (−5)	ND	47.2 cm (−0.4)	51.3 cm (0)
Development and Neurological Data									
Developmental delay	global	global	global	global	global	global	global	global	mild
Hypotonia	yes	yes	yes	yes	yes	yes	yes	no	no
Spasticity	no	no	no	no	yes	yes	yes (legs)	no	no
Sitting (age)	yes (1 year)	no	no	no	yes (1 year)[f]	no	yes (1.5 years)	yes (1 year)	yes (7 months)
Walking (age)	yes (3 years)	no	no	no	yes (5 years)	no	yes (7 years)[g]	yes (3 years)[h]	yes (1.5 years)
Language (age)	>40 words[i]	10 syllables	none[j]	none	3 words[k]	3 words[k]	none	none	yes (1.5 years)
Intellectual disability	severe	severe	severe	severe	severe	severe	severe	severe	severe
Seizure onset	5 months	6 months	3 months	3 months	7 months	5 months	6 months	5 years	4 years, 3 months
Seizure types	ISS	ISS, LGS	SE, LGS	MYO	FSIA, LGS	FSIA, FTCS, GTCS	probable GTCS	MYO, GTCS	FSIA, GTCS
Dyskinesia[l]	hand flapping	mixed	ND	no	mixed	mixed	mixed	hand waving	no
Vision abnormalities	CVI, left ONH	no	CVI	no	normal	normal	ND	ND	normal
Eye movements	abnormal NOS	abnormal NOS	normal	no	nystagmus horizontal	ND	slow tracking	abduction limited[m]	normal
Strabismus	left exotropia	exotropia	ND	no	ND	esotropia	ND	ND	no
Feeding abnormality	none	impaired, GT	impaired, GT	no	ND	ND	none	none	no

(*Continued on next page*)

Table 2. Continued

| Subject ID | LIS with Brainstem Hypoplasia and Dysplasia | | | | | | | | LIS Only |
	LR14-088	LR17-434	LR16-306	LR17-450	LR04-067a1	LR04-067a2	LR18-077	LR18-070[4]	LR16-412
Other									
Feature	VSD closed	none	none	none	none	none	dysmorphic[n]	none	none

Abbreviations are as follows: A, Asian; C, Caucasian; CVI, cortical visual impairment; FSIA, focal seizure with impaired awareness; FTCS, focal tonic-clonic seizure; GT, gastrostomy tube; GTCS, generalized tonic-clonic seizure; ISS, infantile spasm; LGS, Lennox-Gastaut epilepsy syndrome with atonic, tonic, tonic-clonic, and myoclonic seizures; MYO, myoclonic seizure; ND, no data available; NOS, not otherwise specified; OFC, occipitofrontal circumference; ONH, optic-nerve hypoplasia; SD, standard deviation; VSD, ventriculoseptal defect.

[a]GenBank: NM_012090.5 and transcript MACF1-203 (Ensembl: ENST00000361689.6).

[b]Deletion of exons 58–89 (p.Ala3540_Arg5192; GenBank: NM_012090.5) or exons 62–93 (p.Ala5498_Arg7150; MACF1-204).

[c]Transcript MACF1-204 (Ensembl: ENST00000372915.7).

[d]OFC at 36 weeks of gestation.

[e]OFC at 1 year.

[f]Sits with support only.

[g]Few steps only.

[h]Walks with support at 3 years.

[i]Also with several word combinations.

[j]Uses Picture Exchange Communication System (PECS).

[k]Words later lost.

[l]Mixed abnormal movements with combinations of chorea, athetosis, dystonia, and (in the twins) ballismus.

[m]Ocular abduction limited to half normal excursion at 2.5 years but improved to normal abduction by 5 years.

[n]Hypertelorism, low nasal bridge, epicanthal folds, and low-set ears.

Overlapping Phenotypes

Prior ROBO3- and DCC-associated brainstem malformations associated with deficits in midline crossing have been described as "butterfly-like," referring to axial images through the low brainstem (OMIM: 617542 and 607313).[11–14] The W-shaped brainstem phenotype associated with MACF1 mutations affecting the zinc-binding pocket is more severe than the "butterfly" configuration. The midline is very narrow and shows a cleft in MRI from individuals with mutations of all three genes. In addition, the medulla and pons are very narrow and wide in subjects with MACF1 mutations, which is not the case in subjects with ROBO3 or DCC mutations. In some of our subjects, the low brainstem resembles bird wings when inverted (Figure S5), but we did not find this (or really the butterfly-like shape with ROBO3 or DCC mutations) consistent enough to support its use. Mutations in DCC are also associated with severe hypoplasia of the anterior commissure and variable agenesis of the corpus callosum. Bi-allelic mutations in ARHGEF2 have been associated with severe hypoplasia of the transverse pontine crossing fibers and an enlarged medulla, but development of the cerebral commissures and other crossing tracts has not been discussed.[15]

MACF1 in Development

In mice, MACF1 is found in all tissues but most highly in the brain (especially ependymal and mantle layers) and spinal cord.[10] Intermediate amounts are present in the dorsal root ganglia, olfactory epithelium, bronchial epithelium, lung, skeletal muscle, myocardium, and adrenal glands. At embryonic day 12.5 (E12.5), MACF1 is localized widely in the brain and most highly in the ventricular zone, where it co-localizes with Nestin-positive ventricular radial glia cells, and in the upper cortical plate and marginal zone, where it co-localizes with MAP2. By E15.5, MACF1 localization expands to the entire cortical plate and subplate but is reduced in the ventricular and subventricular zones. This pattern fits well with its role in regulating neuronal migration.

Mouse Knockouts

Several homozygous Macf1 loss-of-function (LoF) mouse mutants have been described.[16,17] Complete LoF (Macf1$^{-/-}$) mutant embryos implant and form a neural plate but never develop a primitive streak, node, or axial mesoderm and die at E10.5–E11.5 soon after gastrulation.[9] These features resemble the Wnt3 LoF mutant,[18] which led to studies showing that loss of MACF1 inhibits Wnt signaling via interactions with Axin, GSK3B, APC, LRP5, LRP6, and β-catenin. The binding sites for these interacting proteins are localized to the plakin and spectrin repeat domains of MACF1.[9]

Experiments using embryonic neural drivers (NeuroD6-cre or Nestin-cre) or electroporation of small hairpin antisense RNA to knock down Macf1 demonstrated many developmental defects that resemble the human malformation.[10,16] Mouse mutants had disrupted neuronal migration via disruption of microtubule dynamics and
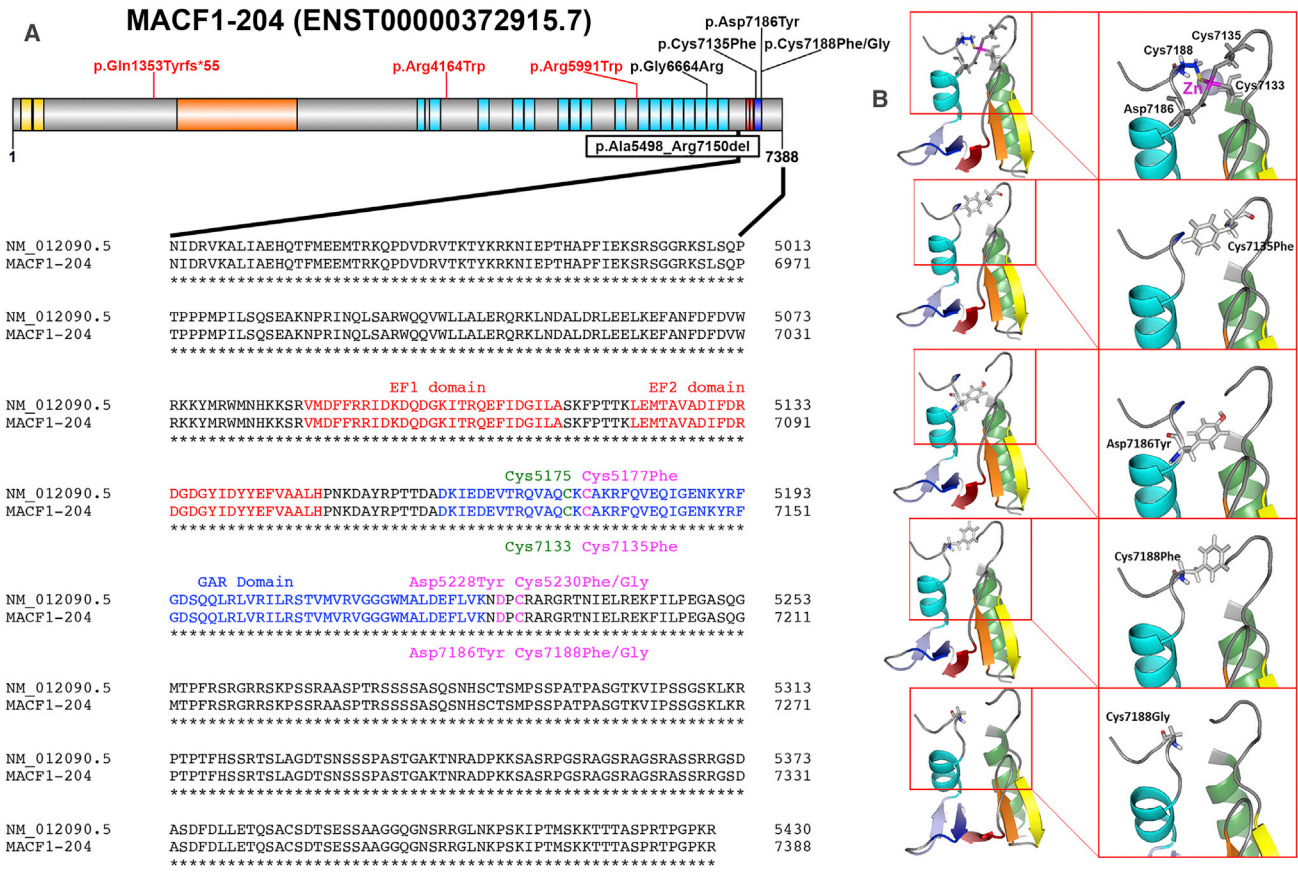
Figure 4. *MACF1* Mutations Affect GAR Domain Amino Acids and Spectrin Rod Repeats

(A) Schematic representation of *MACF1* annotated according to transcript MACF1-204 shows the actin binding Calponin homology domains in yellow, plakin domain in orange, spectrin repeat domains in light blue, EF-hand domains in red, and GAR domain in blue. The missense variants associated with LIS and brainstem hypoplasia (black text) and schizophrenia (red text) are shown above the gene, and the intragenic deletion is shown below the gene. Alignment of the translated protein (GenBank: NM_012090.5) and MACF1-204 (UniProt: Q9UPN3) is shown below the gene. The EF-hand domains are shown in red text, and the zinc-binding GAR domain is shown in blue text. Mutations affecting the residues that coordinate zinc binding (Cys7135, Asp7186, and Cys7188) are shown in magenta above (GenBank: NM_012090.5) or below (UniProt: Q9UPN3) the normal sequence, and the fourth zinc binding residue is shown in green.

(B) 3D models of the four GAR domain missense variants in the PyMOL Molecular Graphics System show significant changes in molecular structure. The top panel shows configuration of the normal GAR domain zinc-binding pocket. The divalent zinc ion is depicted as a gray sphere with a magenta label, and the four residues that coordinate zinc binding are depicted as gray sticks. In the simulated structures with pathogenic variants, the moderate negative charge of cysteine or aspartate is replaced by a bulky hydrophobic residue (phenylalanine or tyrosine; second to fourth panels) or by a small non-polar residue (glycine; bottom panel).

GSK3 signaling, as well as pyramidal neurons throughout the mantle, including the subventricular and ventricular zones, and interneurons found mostly in the intermediate zone.[10,16,19] Some subtypes of radially migrating neurons, including BRN1-, CTIP-, and TBR1-positive neurons, were distributed evenly throughout the mutant cortical plate; conversely, in control brains, they were predominately localized to higher cortical layers. *Macf1*-deleted neurons had short, unstable leading processes, centrosomes that failed to move into the leading process, and unstable microtubules, resulting in unidirectional and slow radial migration. Similar defects were seen in the developing hippocampus.

Mouse knockouts also had abnormal axonal extension and guidance, including multiple defects in midline crossing. The anterior and hippocampal commissures were severely hypoplastic, and the corpus callosum had reduced numbers of fibers.[16] Thalamocortical fiber tracts were thinner and less compact than in control animals and had many fibers misdirected tangentially toward the cortical surface. In addition, a recent transposon-mediated mutagenesis screen using *in utero* electroporation of mouse embryos to detect mutant neural progenitor (radial glia) cells unable to migrate to the cortex identified 33 candidate genes for malformations of cortical development, one of which was *Macf1*.[20]

Defects in axonal extension and guidance have also been seen with mutations in *Short stop* (*shot*), the *Drosphila MACF1* homolog that interacts with Robo and Slit and regulates midline axon crossing.[21] In *shot* mutants, axonal growth cones initiate at the normal time and have normal morphology, including normal axon orientation and fasciculation. However, sensory and (to a lesser extent) motor axons extend only a short distance beyond the cell body.[22]

Heterozygous *MACF1* LoF Could Be Non-pathogenic

The ExAC Browser includes 14 high- and another 26 low-confidence LoF *MACF1* variants, including 19 stop-gained, 16 frameshift, and 5 splice-donor variants. These data imply that heterozygous LoF variants are not pathogenic, even though genome-wide analysis suggested that *MACF1* is highly intolerant to LoF mutations (it ranks seventh most intolerant of 18,225 genes studied; pLI = 1.0).[23]

Alternatively, LoF variants could contribute to neurodevelopmental disorders with incomplete penetrance, given that sequencing studies in three schizophrenia cohorts reported heterozygous *de novo* *MACF1* variants, including one frameshift variant that truncates the protein in the plakin domain and two missense variants in the N-terminal spectrin repeat domain, in three individuals (Table S2 and Figure 4A).[24–26] Both missense variants are located in a MACF1 region that interacts with GSK3B and other proteins known to regulate neuronal migration.[9,10] Notably, several genome-wide association studies have implicated other genes that regulate neuronal migration in the pathogenesis of schizophrenia, such as *DISC1*, *NRG1*, and *RELN*.[27–30] In addition, several reports have described localized malformations of neuronal migration involving entorhinal cortex and subcortical white matter in brains of individuals with schizophrenia.[31,32]

Given that the missense variants we report here cause a more severe phenotype (LIS plus midline-crossing defects) than truncations (non-pathogenic or possibly increased risk of schizophrenia), we hypothesize that the variants in the GAR domain act via either altered function (selective loss or gain of function) or a dominant-negative mechanism.

Although not clearly germane to our findings, two prior studies have suggested a link between *MACF1* or its chromosomal region and other human disorders. In the first, a boy with diffuse hypotonia from infancy was found to have a partial duplication of chromosomal region 1p34.3 involving more than half of the 3' end of *MACF1*. His mother and two full sisters also carried the duplication; all duplication carriers had hypotonia, which varied significantly in severity.[33] In the second study, a candidate-gene study of 105 SNPs across *MACF1* in 713 families affected by Parkinson disease showed a significant association with a single SNP in the region (dbSNP: rs12118033).[34]

Summary

We have identified recurrent *de novo*, heterozygous, missense mutations that involve the zinc ion-binding pocket in the GAR domain of MACF1 and cause defects (resembling those in mouse knockouts) in neuronal migration and axonal pathfinding. In addition, we found that one variant in the spectrin rod domain leads to a neuronal migration defect only. Defining the spectrum of mutations and associated phenotypes will require the discovery of additional mutations in this large and functionally important gene.

Web Resources

CADD version 1.3, http://cadd.gs.washington.edu/home
dbSNP, https://www.ncbi.nlm.nih.gov/projects/SNP/
Ensembl, https://useast.ensembl.org/index.html
ExAC Browser, http://exac.broadinstitute.org
GenBank, https://www.ncbi.nlm.nih.gov/genbank/
gnomAD, http://gnomad.broadinstitute.org
OMIM, http://omim.org/
UniProt, http://www.uniprot.org/

References

1. Goryunov, D., and Liem, R.K. (2016). Microtubule-actin cross-linking factor 1: domains, interaction partners, and tissue-specific functions. Methods Enzymol. *569*, 331–353.

2. Moffat, J.J., Ka, M., Jung, E.M., Smith, A.L., and Kim, W.Y. (2017). The role of MACF1 in nervous system development and maintenance. Semin. Cell Dev. Biol. *69*, 9–17.

3. Lane, T.R., Fuchs, E., and Slep, K.C. (2017). Structure of the ACF7 EF-hand-GAR module and delineation of microtubule binding determinants. Structure *25*, 1130–1138.e6.

4. Irahara, K., Saito, Y., Sugai, K., Nakagawa, E., Saito, T., Komaki, H., Nakata, Y., Sato, N., Baba, K., Yamamoto, T., et al. (2014). Pontine malformation, undecussated pyramidal tracts, and regional polymicrogyria: a new syndrome. Pediatr. Neurol. *50*, 384–388.

5. Di Donato, N., Chiari, S., Mirzaa, G.M., Aldinger, K., Parrini, E., Olds, C., Barkovich, A.J., Guerrini, R., and Dobyns, W.B. (2017). Lissencephaly: expanded imaging and clinical classification. Am. J. Med. Genet. A. *173*, 1473–1488.

6. May-Simera, H.L., Gumerson, J.D., Gao, C., Campos, M., Cologna, S.M., Beyer, T., Boldt, K., Kaya, K.D., Patel, N., Kretschmer, F., et al. (2016). Loss of MACF1 abolishes ciliogenesis and disrupts apicobasal polarity establishment in the retina. Cell Rep. *17*, 1399–1413.

7. Reiter, J.F., and Leroux, M.R. (2017). Genes and molecular pathways underpinning ciliopathies. Nat. Rev. Mol. Cell Biol. *18*, 533–547.

8. Kheradmand Kia, S., Verbeek, E., Engelen, E., Schot, R., Poot, R.A., de Coo, I.F., Lequin, M.H., Poulton, C.J., Pourfarzad, F., Grosveld, F.G., et al. (2012). RTTN mutations link primary cilia function to organization of the human cerebral cortex. Am. J. Hum. Genet. *91*, 533–540.

9. Chen, H.J., Lin, C.M., Lin, C.S., Perez-Olle, R., Leung, C.L., and Liem, R.K. (2006). The role of microtubule actin cross-linking factor 1 (MACF1) in the Wnt signaling pathway. Genes Dev. *20*, 1933–1945.

10. Ka, M., Jung, E.M., Mueller, U., and Kim, W.Y. (2014). MACF1 regulates the migration of pyramidal neurons via microtubule dynamics and GSK-3 signaling. Dev. Biol. *395*, 4–18.

11. Jen, J.C., Chan, W.M., Bosley, T.M., Wan, J., Carr, J.R., Rüb, U., Shattuck, D., Salamon, G., Kudo, L.C., Ou, J., et al. (2004). Mutations in a human ROBO gene disrupt hindbrain axon pathway crossing and morphogenesis. Science *304*, 1509–1513.

12. Hackenberg, A., Boltshauser, E., Gerth-Kahlert, C., Stahr, N., Azzarello-Burri, S., and Plecko, B. (2017). Horizontal gaze palsy in two brothers with compound heterozygous ROBO3 gene mutations. Neuropediatrics *48*, 57–58.

13. Jamuar, S.S., Schmitz-Abe, K., D'Gama, A.M., Drottar, M., Chan, W.M., Peeva, M., Servattalab, S., Lam, A.N., Delgado, M.R., Clegg, N.J., et al. (2017). Biallelic mutations in human DCC cause developmental split-brain syndrome. Nat. Genet. *49*, 606–612.

14. Sicotte, N.L., Salamon, G., Shattuck, D.W., Hageman, N., Rüb, U., Salamon, N., Drain, A.E., Demer, J.L., Engle, E.C., Alger, J.R., et al. (2006). Diffusion tensor MRI shows abnormal brainstem crossing fibers associated with ROBO3 mutations. Neurology *67*, 519–521.

15. Ravindran, E., Hu, H., Yuzwa, S.A., Hernandez-Miranda, L.R., Kraemer, N., Ninnemann, O., Musante, L., Boltshauser, E., Schindler, D., Hübner, A., et al. (2017). Homozygous ARHGEF2 mutation causes intellectual disability and midbrain-hindbrain malformation. PLoS Genet. *13*, e1006746.

16. Goryunov, D., He, C.Z., Lin, C.S., Leung, C.L., and Liem, R.K. (2010). Nervous-tissue-specific elimination of microtubule-actin crosslinking factor 1a results in multiple developmental defects in the mouse brain. Mol. Cell. Neurosci. *44*, 1–14.

17. Wu, X., Kodama, A., and Fuchs, E. (2008). ACF7 regulates cytoskeletal-focal adhesion dynamics and migration and has ATPase activity. Cell *135*, 137–148.

18. Liu, P., Wakamiya, M., Shea, M.J., Albrecht, U., Behringer, R.R., and Bradley, A. (1999). Requirement for Wnt3 in vertebrate axis formation. Nat. Genet. *22*, 361–365.

19. Ka, M., Moffat, J.J., and Kim, W.Y. (2017). MACF1 controls migration and positioning of cortical GABAergic interneurons in mice. Cereb. Cortex *27*, 5525–5538.

20. Lu, I.L., Chen, C., Tung, C.Y., Chen, H.H., Pan, J.P., Chang, C.H., Cheng, J.S., Chen, Y.A., Wang, C.H., Huang, C.W., et al. (2018). Identification of genes associated with cortical malformation using a transposon-mediated somatic mutagenesis screen in mice. Nat. Commun. *9*, 2498.

21. Lee, S., Nahm, M., Lee, M., Kwon, M., Kim, E., Zadeh, A.D., Cao, H., Kim, H.J., Lee, Z.H., Oh, S.B., et al. (2007). The F-actin-microtubule crosslinker Shot is a platform for Krasavietz-mediated translational regulation of midline axon repulsion. Development *134*, 1767–1777.

22. Lee, S., and Kolodziej, P.A. (2002). Short Stop provides an essential link between F-actin and microtubules during axon extension. Development *129*, 1195–1204.

23. Lek, M., Karczewski, K.J., Minikel, E.V., Samocha, K.E., Banks, E., Fennell, T., O'Donnell-Luria, A.H., Ware, J.S., Hill, A.J., Cummings, B.B., et al.; Exome Aggregation Consortium (2016). Analysis of protein-coding genetic variation in 60,706 humans. Nature *536*, 285–291.

24. Kenny, E.M., Cormican, P., Furlong, S., Heron, E., Kenny, G., Fahey, C., Kelleher, E., Ennis, S., Tropea, D., Anney, R., et al. (2014). Excess of rare novel loss-of-function variants in synaptic genes in schizophrenia and autism spectrum disorders. Mol. Psychiatry *19*, 872–879.

25. Wang, Q., Li, M., Yang, Z., Hu, X., Wu, H.M., Ni, P., Ren, H., Deng, W., Li, M., Ma, X., et al. (2015). Increased co-expression of genes harboring the damaging de novo mutations in Chinese schizophrenic patients during prenatal development. Sci. Rep. *5*, 18209.

26. Xu, B., Ionita-Laza, I., Roos, J.L., Boone, B., Woodrick, S., Sun, Y., Levy, S., Gogos, J.A., and Karayiorgou, M. (2012). De novo gene mutations highlight patterns of genetic and neural complexity in schizophrenia. Nat. Genet. *44*, 1365–1369.

27. Ekelund, J., Lichtermann, D., Hovatta, I., Ellonen, P., Suvisaari, J., Terwilliger, J.D., Juvonen, H., Varilo, T., Arajärvi, R., Kokko-Sahin, M.L., et al. (2000). Genome-wide scan for schizophrenia in the Finnish population: evidence for a locus on chromosome 7q22. Hum. Mol. Genet. *9*, 1049–1057.

28. Shifman, S., Johannesson, M., Bronstein, M., Chen, S.X., Collier, D.A., Craddock, N.J., Kendler, K.S., Li, T., O'Donovan, M., O'Neill, F.A., et al. (2008). Genome-wide association identifies a common variant in the reelin gene that increases the risk of schizophrenia only in women. PLoS Genet. *4*, e28.

29. Hodgkinson, C.A., Goldman, D., Jaeger, J., Persaud, S., Kane, J.M., Lipsky, R.H., and Malhotra, A.K. (2004). Disrupted in schizophrenia 1 (DISC1): association with schizophrenia, schizoaffective disorder, and bipolar disorder. Am. J. Hum. Genet. *75*, 862–872.

30. Li, D., Collier, D.A., and He, L. (2006). Meta-analysis shows strong positive association of the neuregulin 1 (NRG1) gene with schizophrenia. Hum. Mol. Genet. *15*, 1995–2002.

31. Muraki, K., and Tanigaki, K. (2015). Neuronal migration abnormalities and its possible implications for schizophrenia. Front. Neurosci. *9*, 74.

32. Yang, Y., Fung, S.J., Rothwell, A., Tianmei, S., and Weickert, C.S. (2011). Increased interstitial white matter neuron density in the dorsolateral prefrontal cortex of people with schizophrenia. Biol. Psychiatry *69*, 63–70.

33. Jørgensen, L.H., Mosbech, M.B., Færgeman, N.J., Graakjaer, J., Jacobsen, S.V., and Schrøder, H.D. (2014). Duplication in the microtubule-actin cross-linking factor 1 gene causes a novel neuromuscular condition. Sci. Rep. *4*, 5180.

34. Wang, X., Li, N., Xiong, N., You, Q., Li, J., Yu, J., Qing, H., Wang, T., Cordell, H.J., Isacson, O., et al. (2017). Genetic variants of microtubule actin cross-linking factor 1 (MACF1) confer risk for Parkinson's disease. Mol. Neurobiol. *54*, 2878–2888.

Supplemental Data

MACF1 Mutations Encoding Highly Conserved

Zinc-Binding Residues of the GAR Domain Cause

Defects in Neuronal Migration and Axon Guidance

William B. Dobyns, Kimberly A. Aldinger, Gisele E. Ishak, Ghayda M. Mirzaa, Andrew E. Timms, Megan E. Grout, Marjolein H.G. Dremmen, Rachel Schot, Laura Vandervore, Marjon A. van Slegtenhorst, Martina Wilke, Esmee Kasteleijn, Arthur S. Lee, Brenda J. Barry, Katherine R. Chao, Krzysztof Szczałuba, Joyce Kobori, Andrea Hanson-Kahn, Jonathan A. Bernstein, Lucinda Carr, Felice D'Arco, Kaori Miyana, Tetsuya Okazaki, Yoshiaki Saito, Masayuki Sasaki, Soma Das, Marsha M. Wheeler, Michael J. Bamshad, Deborah A. Nickerson, University of Washington Center for Mendelian Genomics, Center for Mendelian Genomics at the Broad Institute of MIT and Harvard, Elizabeth C. Engle, Frans W. Verheijen, Dan Doherty, and Grazia M.S. Mancini
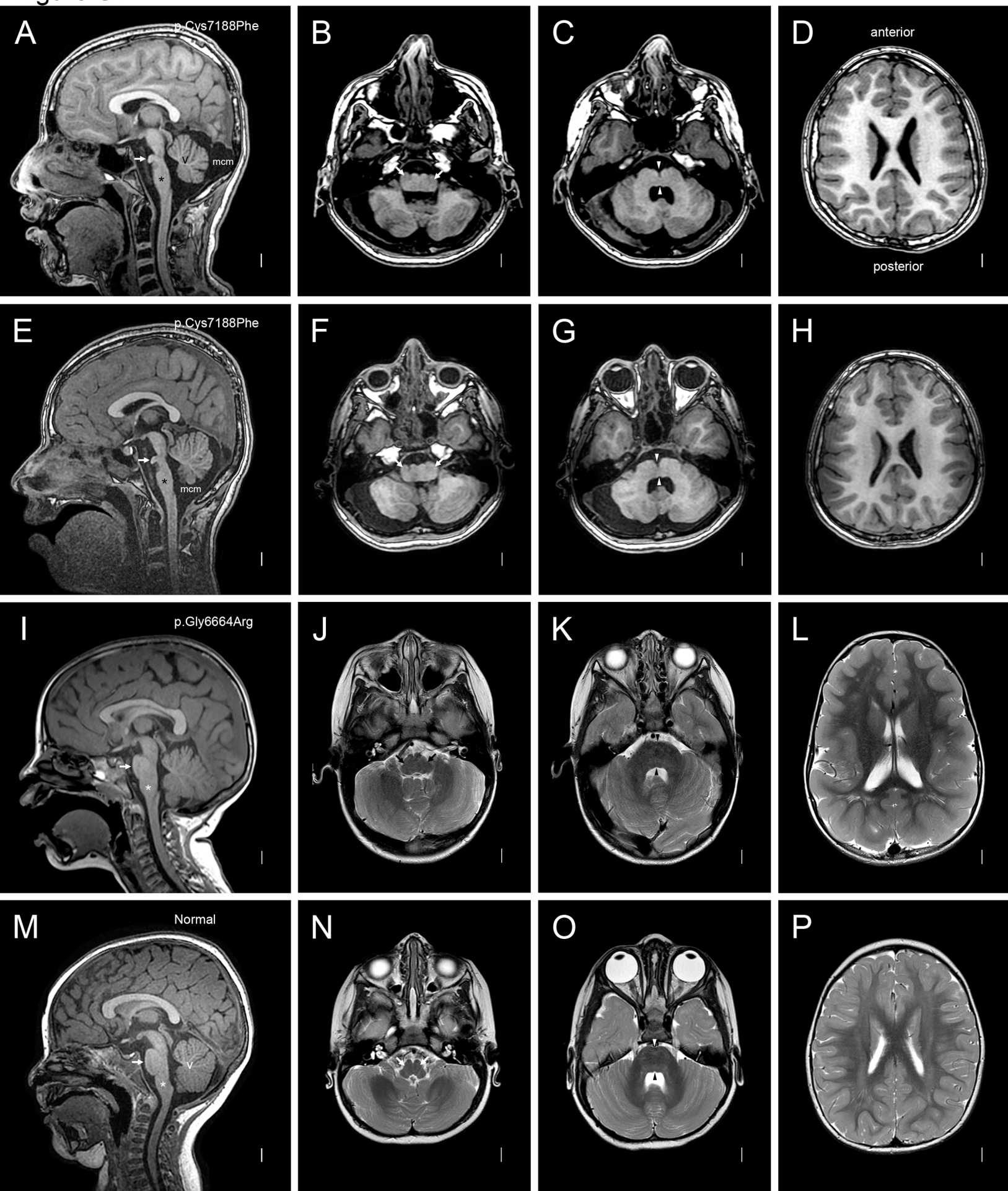
Figure S1

Figure S1. Brain MRI with *MACF1* zinc-binding or rod domain mutations. Images from mid-sagittal (far left column) and three axial planes at the same levels as in Figure 1 are shown from subjects LR04-067a1 (A-D), LR04-067a2 (E-H), LR16-412 (I-L), and a normal control (M-P). *MACF1* mutations are shown in the far left column. Mid-sagittal images from the twins show striking brainstem dysplasia with mildly narrow midbrain, dramatically narrow pons with small but easily seen nodules on the ventral surface (arrows in A, E). The midline images also show borderline vermis hypoplasia (A, E). The medulla is very wide – almost double the typical width – with small pyramids visible on the ventral surface (white arrows in B, F). The pons is very narrow in the midline with a deep ventral cleft (arrowheads in C, G) but also very wide. Corresponding images in the girl with a mutation in the spectrum rod domain appear normal. Higher images in all three subjects including the girl with the rod domain mutation images show diffuse mild pachygyria (D, H) with a posterior more severe than anterior gradient, and only mildly thick cortex (also called "thin" LIS).
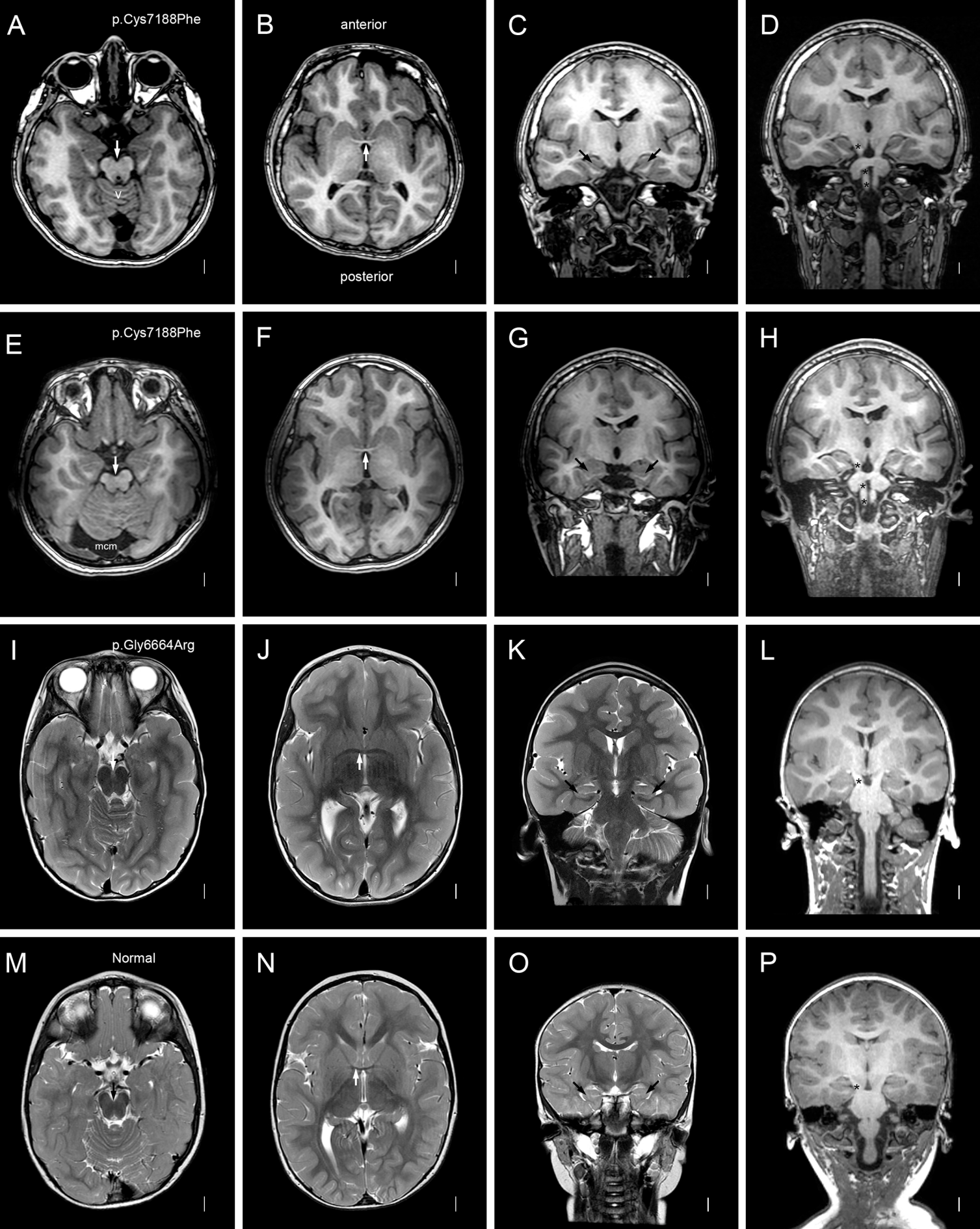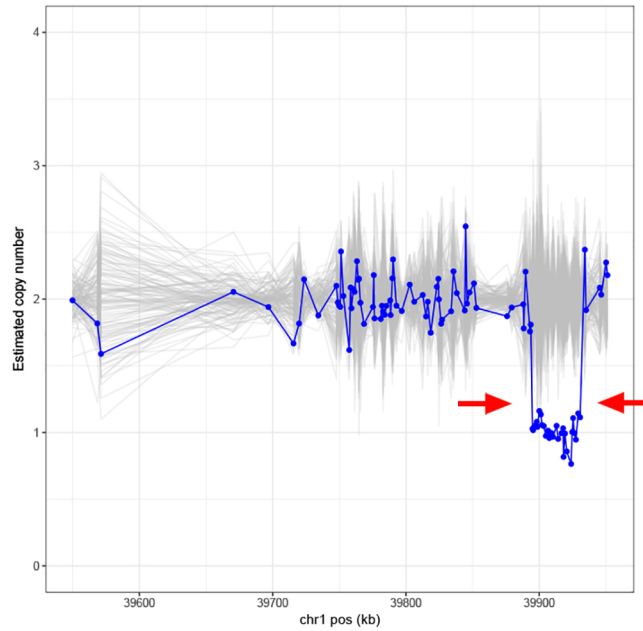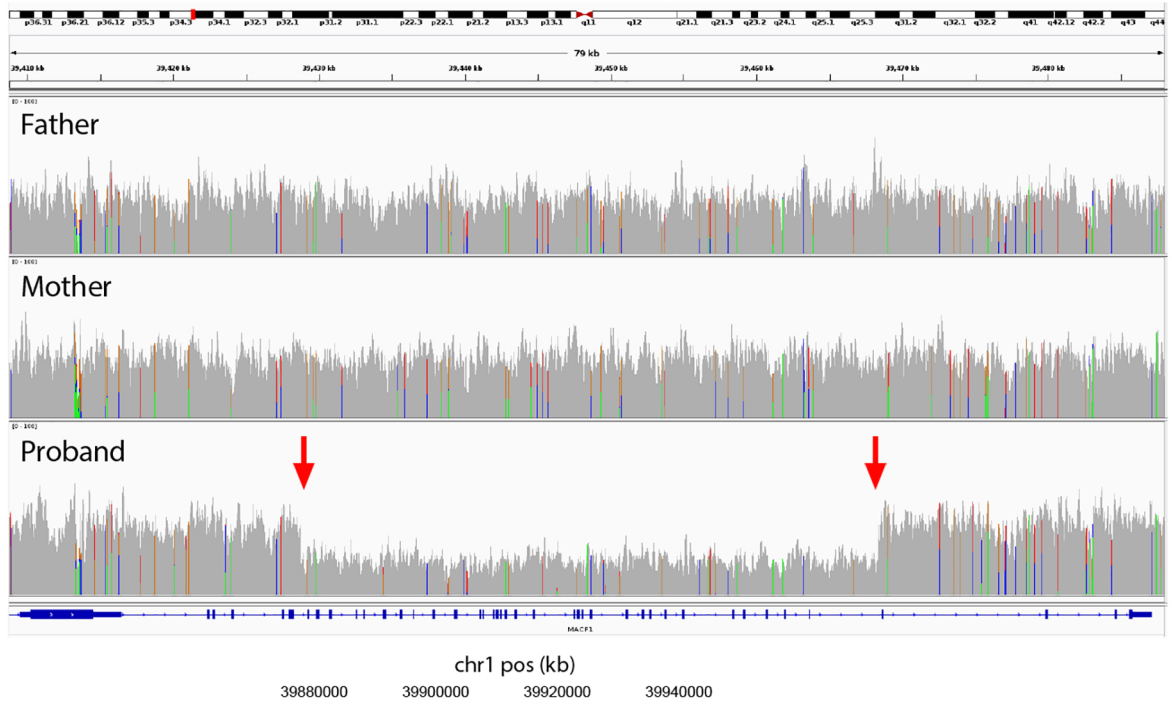
Figure S2

Figure S2. Brain MRI with *MACF1* zinc-binding or rod domain mutations – additional features. Axial (left two columns), coronal (third column), and reconstructed coronal (far right column) images are shown for subjects LR04-067a1 (A-D), LR04-067a2 (E-H), LR16-412 (I-L), and a normal control (M-P). *MACF1* mutations are shown in the far left column. In the top two rows, the low midbrain appears mildly small with no features of the molar tooth malformation (A, E), the anterior commissures are very thin (arrows in B, F), and the hippocampi are small and dysplastic (C, G). The pyramidal tracts are easy to follow (asterisks over the right pyramidal tracts in D, H), although a small bundle of transverse pontine crossing fibers can be seen. Corresponding images for the girl with the rod domain mutation are normal except for borderline thick hippocampi (K). Mild pachygyria (thin LIS) can be seen on all of the axial and coronal images for the three patients (A-L).
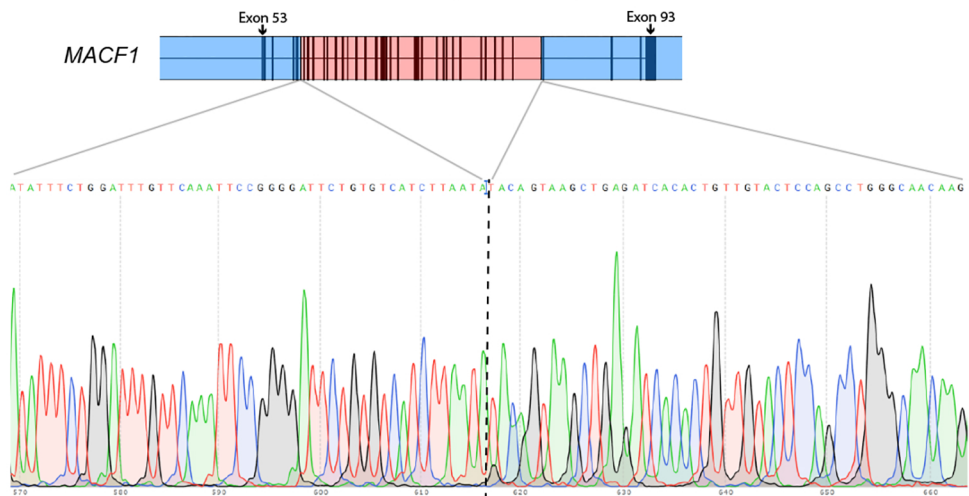
Figure S3

Figure S3. Molecular data supporting an intragenic deletion of *MACF1*. The top panel shows read depth (grey lines) and estimated copy number (blue lines) visualized with the GATK4 GermlineCNVCaller in subject LR18-070 (A). The obvious drop in estimated copy number from 2 to 1 seen just before the 5' end of the gene (red arrows in A) indicates a deletion. The deletion can also be seen in a screen shot from the Integrated Genome Viewer (IGV) using whole genome sequencing data (red arrows in B). A chromatogram from Sanger sequencing with primers on either side of the breakpoint validates location of the breakpoint (dashed vertical line in lower panel in C). Deleted sequence along the *MACF1* gene model (NM_012090.5) is shaded in red while flanking sequence is shaded in blue. Selected exon numbers are denoted by arrows.
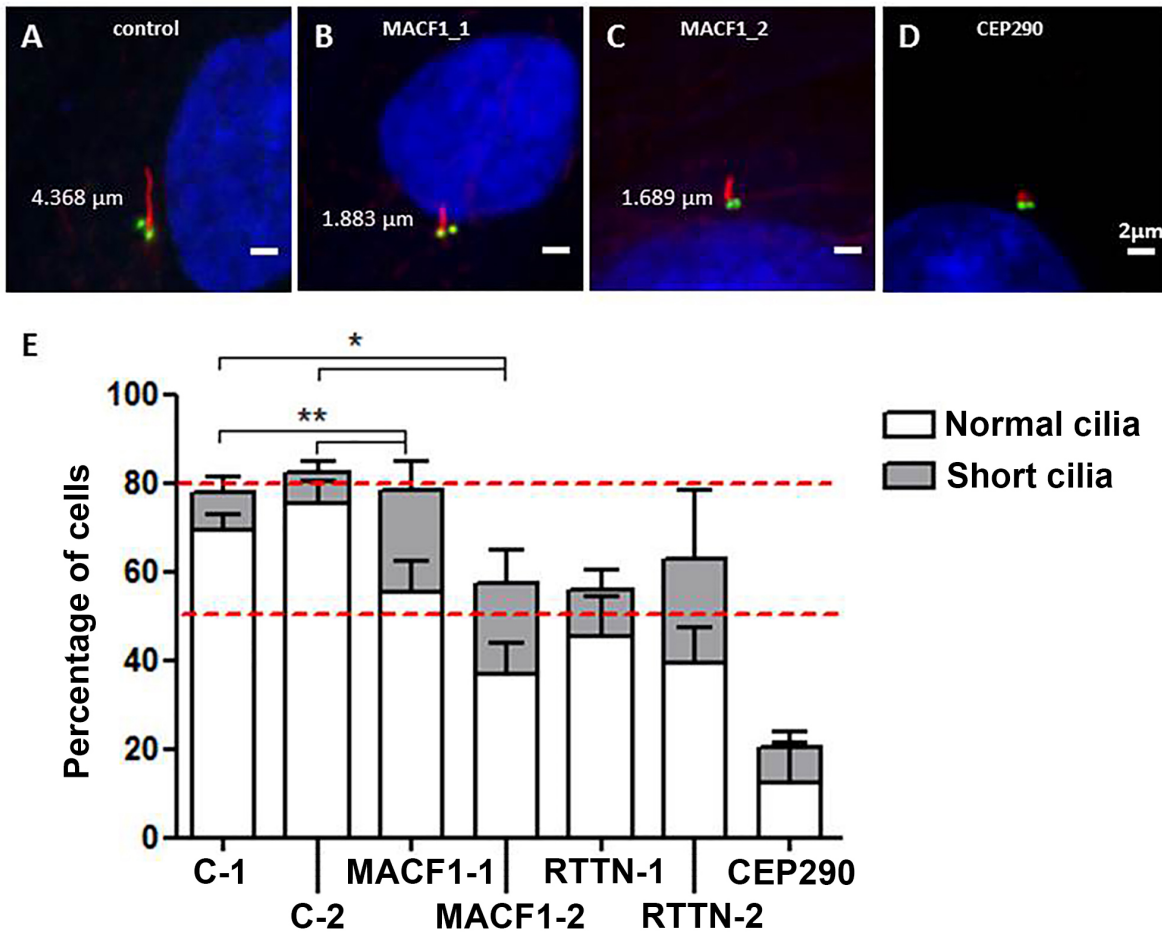
Figure S4

Figure S4. Cilia formation is abnormal with *MACF1* mutations. Formation of cilia was studied in cultured skin fibroblasts following serum starvation and immunostaining with antibodies against gamma-tubulin (basal bodies in green) and acetylated-tubulin (axoneme in red) by measuring both the proportion of cells with cilia and cilia length, with examples of normal (A), short (B, C) and absent (D) cilia shown. Experimental results are shown in a histogram (E) where the Y axis indicates the percentage of total cells in which the basal body has built a primary cilium, and the dark portion of the bars represent cells with an axoneme shorter than 3 μm. Results in two controls, two subjects with heterozygous *MACF1* mutations, two with biallelic *RTTN* mutations, and one with biallelic *CEP290* mutations (along the X axis) show a significant reduction in cilia length in subjects with mutations of *MACF1* or *RTTN*. In contrast, the subject with *CEP290* mutations has severely reduced cilia number. The normal range for ciliation rate (50-80%, dashed red lines) was determined from ~100 experiments using several different control fibroblast lines. Values indicate average plus standard error of the mean (SEM) for separate duplicate or quadruplicate experiments. While *Macf1*$^{-/-}$ mouse embryonic fibroblasts (MEFs) generate no cilia and *Macf1*$^{+/-}$ MEFs have normal cilia, we detect a significant ciliogenesis defect in humans with heterozygous *MACF1* mutation in the GAR domain (*p<0.01;

**p<0.001). The mutations include: MACF1-1 (LR17-434) and MACF1-2 (LR14-088), both heterozygous *MACF1*:p.Cys7135Phe de novo; RTTN-1, compound heterozygous *RTTN*:p.His865Arg and p.Glu1397Lysfs*7; RTTN-2, homozygous *RTTN*:p.Leu932Phe; and CEP290 compound heterozygous *CEP290*: p.Glu501* and p.Arg1508*.
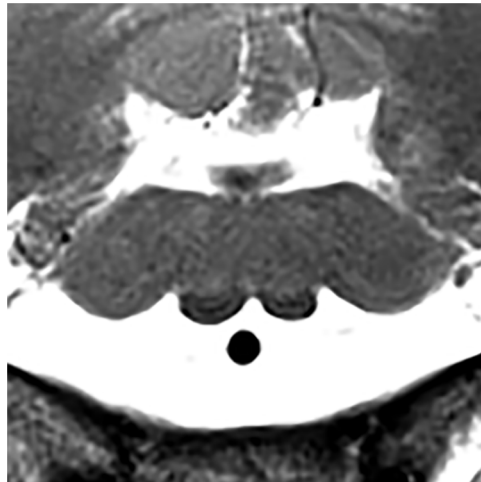
Figure S5

Figure S5. The brainstem malformation may resemble bird wings. Axial images through the medulla when inverted may resemble totem bird wings as shown here for subject LR14-088 (modified from Figure 1B). However, this has not been consistent enough to justify common use.

Table S1. Whole exome and genome sequencing parameters

	LIS with brainstem hypoplasia-dysplasia				
Subject	LR14-088	LR17-434	LR16-306	LR17-450	LR04-067a2
Mutation (MACF1-204)	p.Cys7135Phe	p.Cys7135Phe	p.Asp7186Tyr	p.Asp7186Tyr	p.Cys7188Phe
Testing basis	Research	Clinical	Clinical	Research	Clinical
Testing center	Illumina	ErasmusMC	Baylor	UWCMG	UCGSL
Testing approach	Trio	Trio	Proband	Trio	Trio
NGS type	Exome/Genome	Exome	Exome	Exome	Exome
Capture	NA	SureSelect CRE	SeqCap EZ	Nimblegen_v2	SureSelect
Total reads	997488792	36857470	110212766	60070882	195502268
Total aligned reads (%)	982449620 (98.49%)	36809635 (99,9%)	110099130 (99.90%)	59945462 (99.79%)	192651214 (98.54%)
Median read length	150	150	101	75	150
Mean coverage	46.05	50.05	154.73	53.08	195.35
5X	99.92	97.7	99.42	98.70	97.50%
10X	99.91	96	99.28	96.50	97.30%
20X	99.84	90.4	98.82	88.50	96.50%
50X	33.73	64.8	91.02	47.10	92.50%
Reference for methods	1	2	5	6	4

Abbreviations: NA, not applicable; SureSelect, Illumina SureSelect®; UCGSL, University of Chicago Genetic Services Laboratories; UWCMG, University of Washington Center for Mendelian Genomics. Only Sanger sequencing was performed in subjects LR04-067a1 (twin) and LR18-077.

Table S1, continued

	LIS-brainstem	LIS only
Subject	LR18-070[13]	LR16-412
Mutation (MACF1-204)	Deletion	p.Gly6664Arg
Testing basis	Research	Clinical
Testing center	Broad Institute	GeneDx
Testing approach	Trio	Trio
NGS type	Exome/Genome	Exome
Capture	SureSelect	SureSelect HAE
Total reads	196860614	54873093
Total aligned reads (%)	195183707 (99.1%)	54721312 (99.72%)
Median read length	101	150
Mean coverage	144.98	123.22
5X	NA	98.81
10X	90.37	98.66
20X	88.08	98.10
50X	79.51	91.78
Reference for methods	7	17

Table S2. *MACF1* mutation and protein variant data

Subject ID	Chr	Position [hg19]	Ref	Alt	Transcript NM_012090.5[a]	
					cDNA	Protein
LIS-BSH						
LR14-088	1	g.39929312	G	T	c.15530G>T	p.Cys5177Phe
LR17-434	1	g.39929312	G	T	c.15530G>T	p.Cys5177Phe
LR16-306	1	g.39934392	G	T	c.15682G>T	p.Asp5228Tyr
LR17-450	1	g.39934392	G	T	c.15682G>T	p.Asp5228Tyr
LR18-077	1	g.39934398	T	G	c.15688T>G	p.Cys5230Gly
LR04-067a1[f]	1	g.39934399	G	T	c.15689G>T	p.Cys5230Phe
LR04-067a2[f]	1	g.39934399	G	T	c.15689G>T	p.Cys5230Phe
LR18-070[13]	1	g.39894403[g]	39.6 kb deletion		exon 58-89 deletion[h]	p.Ala3540_Arg5192del
LIS only						
LR16-412	1	g.39916758	G	C	c.14116G>C	p.Gly4706Arg
SCZ only						
Kenny 2014[14]	1	g.39788292[i]	CAAC	TA	c.4057_4060delinsTA	p.Gln1353Tyrfs*55
Wang 2015[15]	1	g.39827053	C	T	c.6289C>T	p.Arg2097Trp
Xu 2012[16]	1	g.39904999	C	T	c.12097C>T	p.Arg4033Trp

Table S2. continued

Subject ID	Transcript MACF1-204[b]		Mutation type[c]	CADD[d]	PolyPhen-2[e]
	cDNA	Protein			
LIS-BSH					
LR14-088	c.21404G>T	p.Cys7135Phe	Missense	34	0.997[j]
LR17-434	c.21404G>T	p.Cys7135Phe	Missense	34	0.997[j]
LR16-306	c.21556G>T	p.Asp7186Tyr	Missense	34	0.999[j]
LR17-450	c.21556G>T	p.Asp7186Tyr	Missense	34	0.999[j]
LR18-077	c.21562T>G	p.Cys7188Gly	Missense	31	0.995[j]
LR04-067a1[d]	c.21563G>T	p.Cys7188Phe	Missense	34	0.997[j]
LR04-067a2[d]	c.21563G>T	p.Cys7188Phe	Missense	34	0.997[j]
LR18-070[13]	exon 62-93 deletion	p.Ala5498_Arg7150del	Deletion (in frame)	NA	--
LIS only					
LR16-412	c.19990G>C	p.Gly6664Arg	Missense	34	0.999[j]
SCZ only					
Kenny 2014[14]	c.4057_4060delinsTA	p.Gln1353Tyrfs*55	Indel	36	--
Wang 2015[15]	c.12490C>T	p.Arg4164Trp	Missense	25	0.022[k]
Xu 2012[16]	c.17971C>T	p.Arg5991Trp	Missense	34	0.993[j]

Abbreviations: Alt, alternate allele; Chr, chromosome; LIS, lissencephaly; NA, not applicable; Ref, reference allele; SCZ, schizophrenia. Footnotes: [a]NCBI Reference Sequence NM_012090.5 and Ensemble Sequence MACF1-203, transcript ID ENST00000361689.6; [b]Ensemble Sequence MACF1-204, transcript ID ENST00000372915.7; [c]Variants were all de novo; [d]CADD version 1.3 (http://cadd.gs.washington.edu/home); [e]Variants were all Not Scored by SIFT; [f]monozygotic twins; [g]g.39894403_39934001del; [h]c.10617+444_15577-288del; [i]g.39788292_39788295delinsTA; [j]probably damaging; [k]benign.

SUPPLEMENTAL METHODS

Participants
Clincal data including brain imaging studies performed as part of routine care were reviewed and summarized (Tables 1-2). Skin biopsies were performed on two children and used to establish fibroblast cultures by standard methods.

Molecular methods
Whole exome and genome sequencing were performed at seven different centers using center specific pipelines as described previously (Table S1).[1-7] The small intragenic deletion found in subject LR18-070 was confirmed in whole genome data using the Manta SV caller,[8] and in whole exome data using the GATK4 GermlineCNVCaller (Box 1).[9] We designed primers flanking the breakpoint (forward primer: CAGGCCCGATACAGTGAAAT; and reverse primer: AACAGACAGACCCCACCATC), and performed PCR under the following conditions: 95°C for 1 min. followed by 35 cycles of 94°C for 10 seconds, 60°C for 10 seconds, and 72°C for 1 second. Sanger sequencing was then performed using these primers.

Protein modeling
The solved structure of the human MACF1 (a.k.a. hACF7) EF1-EF2-GAR domains (5VE9.pdb in the RCSB Protein Data Bank) was loaded in PyMOL Molecular Graphics System (version 1.5.0.5, Schrödinger, LLC).[10; 11] The wild type Cys-Cys-Asp-Cys residues and coordinated zinc ion were visualized as stick models. Simulations of four missense variants in the GAR domain were computed using the PyMOL mutagenesis wizard.

Cilia number and length in cultured fibroblasts
Skin-derived fibroblast cell lines from two control individuals and five subjects with mutations of *MACF1* or two other genes (*RELN*, *CEP290*) known to regulate cilia formation were grown and processed in parallel in duplicate or quadruplicate as previously described.[12]

Immunocytochemisty. Fibroblasts were plated at 5×10^4 cells/cm^2 on 24 mm cover slips (Thermo Fisher Scientific®), and cultured in 2 mL DMEM+/+ (10% Fetal Calf Serum, 1% PenStrep, Lonza®) in a 6 well plate. The next day, cell confluency reached 80% and culture media was replaced with 2mL DMEM-/-. Cells were serum starved for 48 hours to induce ciliogenesis. After fixing cells with methanol for 10 minutes at -20 °C, coverslips were incubated with blocking buffer containing 50mM Tris HCl pH 7.4, 0.9% NaCl, 0.25% gelatin, and 0.5% TritonX-100 for 10 minutes on ice. Primary and secondary antibody dilutions were prepared in blocking buffer. Incubation with primary antibody was done overnight at 4°C. Slips were washed with 1x PBS (Sigma Aldrich®) and incubated with secondary antibody for 1 hour at room temperature. After washing, coverslips were placed on a microscope slide with 20 μL ProLong® Gold Antifade Reagent with DAPI (Thermo Fisher Scientific®) and dried in 37 °C for 4 hours.

Antibodies. Primary antibodies used included mouse monoclonal anti-human acetylated tubulin (Sigma Aldrich® T7451), and rabbit polyclonal anti-human gamma tubulin (Sigma Aldrich® T3320). The secondary antibodies used in a 1 in 10,000 dilution were Green DyLight TM488-

conjugated AffiniPure Donkey Anti-Rabbit IgG, and Red Cy™3 AffiniPure Donkey Anti-Mouse IgG (H+L)(Jackson Laboratories® 715-165-150).

Experimental design. Cells from five individuals with known mutations (*MACF1* x2, *RTTN* x2, *CEP290* x1) and two control lines – were processed in parallel in duplicate or quadruplicate as previously described.[12] Dishes were blinded, and cells with basal bodies (γ-tubulin-positive) were scored for cilia length, defined as normal (>3 µm) or short (<3 µm), in four different quadrants for each coverslip by one individual. Values indicate average +/- SEM. Under these conditions, 50-80% of cells grow cilia based on data from 100 experiments using multiple control fibroblast lines. Statistical tests were performed using Prism 5 GraphPad.

WEB RESOURCES
GATK4 GermlineCNVCaller
    <https://github.com/broadinstitute/gatk/tree/master/scripts/cnv_wdl/germline>
Manta Structural Variant Caller
    <https://github.com/Illumina/manta>

SUPPLEMENTARY REFERENCES

1. Alcantara, D., Timms, A.E., Gripp, K., Baker, L., Park, K., Collins, S., Cheng, C., Stewart, F., Mehta, S.G., Saggar, A., et al. (2017). Mutations of AKT3 are associated with a wide spectrum of developmental disorders including extreme megalencephaly. Brain 140, 2610-2622.
2. Oegema, R., Baillat, D., Schot, R., van Unen, L.M., Brooks, A., Kia, S.K., Hoogeboom, A.J.M., Xia, Z., Li, W., Cesaroni, M., et al. (2017). Human mutations in integrator complex subunits link transcriptome integrity to brain development. PLoS Genet 13, e1006809.
3. Di Gioia, S.A., Connors, S., Matsunami, N., Cannavino, J., Rose, M.F., Gilette, N.M., Artoni, P., de Macena Sobreira, N.L., Chan, W.M., Webb, B.D., et al. (2017). A defect in myoblast fusion underlies Carey-Fineman-Ziter syndrome. Nat Commun 8, 16077.
4. Sun, M., Knight Johnson, A., Nelakuditi, V., Guidugli, L., Fischer, D., Arndt, K., Ma, L., Sandford, E., Shakkottai, V., Boycott, K., et al. (2018 in press). Exome sequencing and targeted analysis identifies the genetic basis of disease in over 50% of patients with a wide range of ataxia-related phenotypes. Genet Med.
5. Yang, Y., Muzny, D.M., Reid, J.G., Bainbridge, M.N., Willis, A., Ward, P.A., Braxton, A., Beuten, J., Xia, F., Niu, Z., et al. (2013). Clinical Whole-Exome Sequencing for the Diagnosis of Mendelian Disorders. N Engl J Med.
6. Van De Weghe, J.C., Rusterholz, T.D.S., Latour, B., Grout, M.E., Aldinger, K.A., Shaheen, R., Dempsey, J.C., Maddirevula, S., Cheng, Y.H., Phelps, I.G., et al. (2017). Mutations in ARMC9, which Encodes a Basal Body Protein, Cause Joubert Syndrome in Humans and Ciliopathy Phenotypes in Zebrafish. Am J Hum Genet 101, 23-36.

7. Poulsen, J.B., Lescai, F., Grove, J., Baekvad-Hansen, M., Christiansen, M., Hagen, C.M., Maller, J., Stevens, C., Li, S., Li, Q., et al. (2016). High-Quality Exome Sequencing of Whole-Genome Amplified Neonatal Dried Blood Spot DNA. PLoS One 11, e0153253.

8. Chen, X., Schulz-Trieglaff, O., Shaw, R., Barnes, B., Schlesinger, F., Kallberg, M., Cox, A.J., Kruglyak, S., and Saunders, C.T. (2016). Manta: rapid detection of structural variants and indels for germline and cancer sequencing applications. Bioinformatics 32, 1220-1222.

9. McKenna, A., Hanna, M., Banks, E., Sivachenko, A., Cibulskis, K., Kernytsky, A., Garimella, K., Altshuler, D., Gabriel, S., Daly, M., et al. (2010). The Genome Analysis Toolkit: a MapReduce framework for analyzing next-generation DNA sequencing data. Genome Res 20, 1297-1303.

10. Alexander, N., Woetzel, N., and Meiler, J. (2011). bcl::Cluster: A method for clustering biological molecules coupled with visualization in the Pymol Molecular Graphics System. IEEE Int Conf Comput Adv Bio Med Sci 2011, 13-18.

11. Lane, T.R., Fuchs, E., and Slep, K.C. (2017). Structure of the ACF7 EF-Hand-GAR Module and Delineation of Microtubule Binding Determinants. Structure 25, 1130-1138 e1136.

12. Kheradmand Kia, S., Verbeek, E., Engelen, E., Schot, R., Poot, R.A., de Coo, I.F., Lequin, M.H., Poulton, C.J., Pourfarzad, F., Grosveld, F.G., et al. (2012). RTTN mutations link primary cilia dunction to organization of the human cerebral cortex. Am J Hum Genet 91, 533-540.

13. Irahara, K., Saito, Y., Sugai, K., Nakagawa, E., Saito, T., Komaki, H., Nakata, Y., Sato, N., Baba, K., Yamamoto, T., et al. (2014). Pontine malformation, undecussated pyramidal tracts, and regional polymicrogyria: a new syndrome. Pediatr Neurol 50, 384-388.

14. Kenny, E.M., Cormican, P., Furlong, S., Heron, E., Kenny, G., Fahey, C., Kelleher, E., Ennis, S., Tropea, D., Anney, R., et al. (2014). Excess of rare novel loss-of-function variants in synaptic genes in schizophrenia and autism spectrum disorders. Mol Psychiatry 19, 872-879.

15. Wang, Q., Li, M., Yang, Z., Hu, X., Wu, H.M., Ni, P., Ren, H., Deng, W., Li, M., Ma, X., et al. (2015). Increased co-expression of genes harboring the damaging de novo mutations in Chinese schizophrenic patients during prenatal development. Sci Rep 5, 18209.

16. Xu, B., Ionita-Laza, I., Roos, J.L., Boone, B., Woodrick, S., Sun, Y., Levy, S., Gogos, J.A., and Karayiorgou, M. (2012). De novo gene mutations highlight patterns of genetic and neural complexity in schizophrenia. Nat Genet 44, 1365-1369.

17. Retterer, K., Juusola, J., Cho, M.T., Vitazka, P., Millan, F., Gibellini, F., Vertino-Bell, A., Smaoui, N., Neidich, J., Monaghan, K.G., et al. (2016). Clinical application of whole-exome sequencing across clinical indications. Genet Med 18, 696-704.